Static Bending Analysis of Foam Filled Orthogonally Rib-Stiffened Sandwich Panels: A Mathematical Model

S. Soleimanian, A. Davar, J. Eskandari Jam [*], M. Heydari Beni

University Complex of Materials and Manufacturing Technology, Malek Ashtar University of Technology, Tehran, Iran

ABSTRACT

The current study presents a mathematical modeling for sandwich panels with foam filled orthogonally rib-stiffened core using Heaviside distribution functions. The governing equations of the static problem have been derived based on classical lamination theory. The present model contains three displacement variables considering all of the stiffness coefficients. A closed form solution using Galerkin's method is presented for simply supported sandwich panels with foam filled orthogonally rib-stiffened core subjected to uniform lateral static pressure. Compared to previous researches, the present work is comprehensive enough to be used for symmetric, unsymmetric, laminated or filament wound panels with orthogrid stiffeners. The accuracy of the solution is checked both through comparisons with previous works, and the results of simulation with ABAQUS software.

© 2019 IAU, Arak Branch. All rights reserved.

Keywords: Composite; Sandwich panels; Grid stiffened; Static bending analysis; Galerkin's method; Heaviside distribution functions.

1 INTRODUCTION

IN order to lighten the weight of structures it is common to make rectangular, circular or other shapes of cutouts in the structures. Lattice and rib-stiffened structures are extensively used to lighten the weight, while saving properties such as stiffness and strength. Analysis of these structures is a challenge for researchers, due to the presence of geometry gaps. The related literature especially those aim at methods considering the effects of geometrical discontinuities such as voids, cutouts and stiffeners, to physical or mechanical properties of structures are presented herein. Yettram and Brown [1] studied the elastic stability of square perforated plates subjected to bi-axial loading using a finite difference method. Choi et al. [2] investigated modal analysis of free edged perforated plates using finite element method (FEM) and experiment. In the FEM model, they investigated the accuracy of results based on equivalent elastic properties for perforated plates. As the first attempt on analytical modeling of isotropic plates with voids, Takabatake [3] presented a material modeling using the unit step function to define the structure stiffness. For static analysis, he used Galerkin's method to solve the differential equation of equilibrium. Rezaeepazhand and Jafari [4] presented an analytical solution for stress analysis of composite plates with various

_____

[*]Corresponding author.
E-mail address: jejaam@gmail.com (J. Eskandari Jam).

shapes central cutout (square, circular, triangular and hexagonal) using a general mapping function. They investigated the effect of material properties, effect of bluntness and fiber orientation. They proclaimed that the method is suitable to change the stress concentration of perforated plates significantly. Li and Cheng [5] analysed grid stiffened composite sandwich panels with simply supported edges subjected to lateral uniform pressure. For an orthogrid-stiffened plate, they considered two material regions, the cell and the surrounding ribs. Based on this concept, they modeled the grid shape in terms of Heaviside functions, which results local definition for *ABD* matrices. The governing equations are solved by considering only the normal component of displacement, so the solution is limited to symmetric sandwich lay-ups. Huang et al. [6] presented a general FEM model using triangular curved shell element for buckling of grid stiffened laminated plates with arbitrary stiffening configurations. They successfully used their model to investigate the effect of number of plies for stiffener and skin plate. Furthermore, they studied the effect of stiffener depth on the buckling response of grid stiffened plates. Wodesenbet et al. [7] developed a smeared method based on the volume fraction of stiffener and shell to find the equivalent stiffness of grid stiffened panels. Legault et al. [8] studied the vibro-acoustic response of orthogonally stiffened panels. Multiplying a correction factor to the transmissibility parameter of a bare panel, they investigated the transmissibility of the orthogrid stiffened panel. Dharshani [9] investigated the deflection and failure of GFRP stiffened composite plates with rectangular cutout subjected to axial and lateral loading by finite element analyses and experiments. Nemeth [10] derived equivalent stiffness and thickness formulations for plates reinforced with orthogrid, star and hexagon cell shaped stiffening grids. Weber and Middendorf [11] performed a geometrical non-dimensionalisation to study the buckling problem of orthotropic grid stiffened shells with different stiffening patterns. Ovesy and Fazilati [12] developed a finite strip method for buckling and free vibration analysis of composite plates with cutout. Qing et al. [13] studied the static and dynamic characteristics of curvilinearly stiffened plates. Using NUBRS (non-uniform rational B-splines) and parametric coordinates, they presented a shape function to define the stiffener geometry. Azhari et al. [14] studied the buckling problem of stepped and perforated plates by defining subregions with different thicknesses using interpolation functions. In another work, Wilson et al. [15] performed a research on elastic stability of stepped and stiffened plates. They modeled structures with variation in thickness such as single stepped, double stepped and latitudinal stiffened plates using piecewise functions for thickness.

According to the review of the literature, there are two main schemes for exact mathematical modeling of structures with voids:
1) Using distribution functions to define the stiffness of the structures.
2) Using distribution functions to define the thickness of the structures.

The first scheme has been followed in Refs. [3, 5,10], and the second scheme is the basis of analytical modeling in Refs. [10,12]. Structures with filled or unfilled voids can be modeled by developing the first scheme, while the second one can be only used for modeling structures with unfilled voids.

The present work deals with a developed mathematical modeling of orthogonal pattern of stiffening ribs that can cover structures made of isotropic, laminated composite and filament wound materials. The mathematical modeling introduces Heaviside distribution functions that make it possible to separate the structure regions by the type of material. The equilibrium equations are derived for a sandwich panel with foam filled orthogonally rib-stiffened core subjected to lateral pressure load based on classical lamination theory. The equations are solved by performing closed form Galerkin's method considering simply supported boundary conditions. The solution procedure is performed using a MATLAB code including symbolic operations. The accuracy of theoretical modeling is checked through comparisons with available literature data and FEM modeling.

2 PROBLEM DEFINITION

As shown in Fig. 1 a sandwich panel composed of three layers, an orthogonally stiffened core filled with an isotropic filler material and two face sheets attached to the top and bottom sides is studied in this work. The plate lies in the region $0 \le x \le a, \ 0 \le y \le b, \ -\frac{h}{2} \le z \le \frac{h}{2}$ according to the coordinate system placed on the middle surface of the sandwich panel. The core and the face sheets thicknesses can take different values, so that the surface $z=0$ passes through the middle of the total structure thickness. The parameters t_c, t_{s1} and t_{s2} are the thicknesses of the core layer, upper and lower face sheets, respectively.
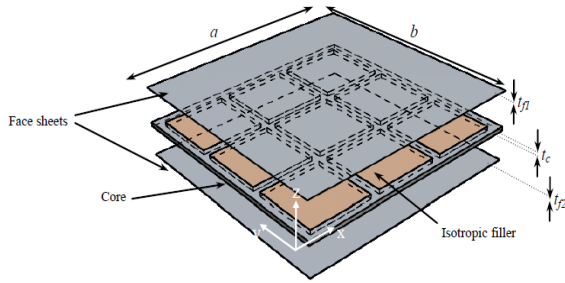
Fig.1
Sandwich panel with orthogrid core and facesheets.

The foam filled orthogonally rib-stiffened core can be modeled by considering two or four material regions. When the core plate is made of metals, laminated composites or any other common industrial material it possesses two material regions, ribs and cells (see Fig. 2(a)) and when it is made with filament winding process, the structure possesses four material regions, horizontal ribs (0° ribs), vertical ribs (90° ribs), intersection regions and cells (see Fig. 2(b)). The parameters *c* and *d* are the length and width of the cells, respectively.

Filament wound stiffened composites are well known due to their high specific strength and stiffness [16]. Filament winding process for fabrication of these structures is such that resin-impregnated unidirectional fibers are placed in orthogonal directions layer by layer. In an orthogonally rib-stiffened plate, the number of layers in intersection regions is twice that of those in vertical and horizontal rib regions obviously (see Fig. 2(b)). The unidirectional ribs are the main structural components of the stiffened structure which provide both membrane and bending stiffness, while the filler regions are considered to protect the sandwich panel from buckling and crippling [5, 14].

For filament wound stiffened structures, the fiber volume fraction reported by reference is about 40% in unidirectional ribs and 75% in intersections [16].

(a)   (b)
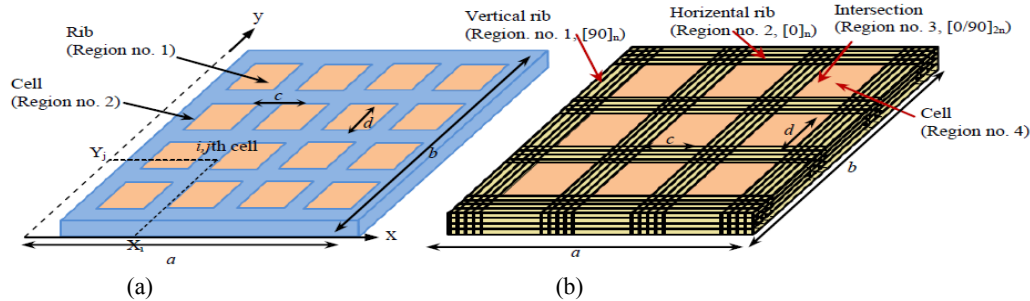
Fig.2
a) Core plate with two material regions. b) Core plate with four material regions (filament wound structure).

2.1 Mathematical modeling

To model the orthogonal pattern of the stiffening ribs mathematically, the Heaviside distribution functions HD_x and HD_y are introduced by Eqs. (1a) and (1b), respectively. HD_x and HD_y functions produce the orthogonal pattern by creating specific divisions in the x and y directions, respectively. Number of the produced cells in x and y directions are considered m_x and n_y, respectively.

$$HD_x = \sum_{i=1}^{m_x} \sum_{j=1}^{n_y} \left(Heaviside\left(x - X_i + \frac{c}{2}\right) - Heaviside\left(x - X_i - \frac{c}{2}\right)\right) \tag{1a}$$

$$HD_y = \sum_{i=1}^{m_x} \sum_{j=1}^{n_y} \left(Heaviside\left(y - Y_i + \frac{d}{2}\right) - Heaviside\left(y - Y_i - \frac{d}{2}\right)\right) \tag{1b}$$

where (X_i, Y_j) is the coordinate of the center of cells.

The stiffness of a foam filled orthogonally rib-stiffened core considering two material regions can be written as:

$$Q = Q^{rib}\left(1 - HD_x, HD_y\right) + Q^{cell}\left(HD_x, HD_y\right) \tag{2}$$

Eq. (2) is reported in Ref. [5] where Q^{rib} and Q^{cell} are the stiffness of the ribs and the cells, respectively. The stiffness of a foam filled orthogonally rib-stiffened fillament wound core can be obtained by the developed mathematical model given by Eq. (3).

$$Q = Q^0\left(1 - HD_y\right)\left(HD_x - HD_y\right) + Q^{90}\left(1 - HD_x\right)\left(HD_y - HD_x\right) + Q^i\left(1 - HD_y\right)\left(1 - HD_x\right) + Q^{cell}\left(HD_x, HD_y\right) \tag{3}$$

Q^0, Q^{90} and Q^i are the stiffness of the 0° ribs, 90° ribs and the intersection regions, respectively. Whether the core plate is made of two material regions or four ones, the stiffness of cells and 0° ribs can be given by Eq. (4) using engineering constants [17].

$$Q^k = \begin{bmatrix} \dfrac{E_1}{1 - \upsilon_{12}\upsilon_{21}} & \dfrac{\upsilon_{12}E_2}{1 - \upsilon_{12}\upsilon_{21}} & 0 \\ \dfrac{\upsilon_{21}E_1}{1 - \upsilon_{12}\upsilon_{21}} & \dfrac{E_2}{1 - \upsilon_{21}\upsilon_{12}} & 0 \\ 0 & 0 & G_{12} \end{bmatrix} \tag{4}$$

and the stiffness of 90° ribs can be given by Eq. (5).

$$Q^k = \begin{bmatrix} \dfrac{E_2}{1 - \upsilon_{21}\upsilon_{12}} & \dfrac{\upsilon_{21}E_1}{1 - \upsilon_{12}\upsilon_{21}} & 0 \\ \dfrac{\upsilon_{12}E_2}{1 - \upsilon_{12}\upsilon_{21}} & \dfrac{E_1}{1 - \upsilon_{12}\upsilon_{21}} & 0 \\ 0 & 0 & G_{12} \end{bmatrix} \tag{5}$$

Since in a filament wound structure, the intersection regions are cross-ply laminates, the stiffness of each layer (Q^i) should be considered in derivation of *ABD* formuals given in Section 2.4.

2.2 Strain-displacement relations

According to the classical lamination theory and Kirchoff's hypothesis, the displacements of the plate can be expressed as [18]:

$$u\left(x, y, z\right) = u_0\left(x, y\right) - z w_{(0,x)}\left(x, y\right) \tag{6}$$

$$\upsilon\left(x, y, z\right) = \upsilon_0\left(x, y\right) - z w_{(0,y)}\left(x, y\right) \tag{7}$$

$$w\left(x, y, z\right) = w_{(0)}\left(x, y\right) \tag{8}$$

The midplane strains are:

$$\varepsilon_{0,x} = u_{0,x} \tag{9}$$

$$\varepsilon_{0,y} = u_{0,y} \tag{10}$$

$$\gamma_{0,y} = u_{0,y} + \upsilon_{0,x} \tag{11}$$

and the midplane curvatures are:

$$k_x = -w_{0,xx} \tag{12}$$

$$k_y = -w_{0,yy} \tag{13}$$

$$k_{xy} = -2w_{0,xy} \tag{14}$$

2.3 Governing equations of rectangular sandwich panel

Using the Hamilton's principle, equilibrium equations of a sanwich panel are as follows [18]:

$$N_{x,x} + N_{xy,y} = 0 \tag{15}$$

$$N_{xy,x} + N_{y,y} = 0 \tag{16}$$

$$M_{xx,x} + 2M_{xy,xy} + M_{y,yy} + p = 0 \tag{17}$$

where the parameter *p* is the lateral pressure applied as an external excitation. Force and moment resultants are given by [17]:

$$\begin{bmatrix} N \\ M \end{bmatrix} = \begin{bmatrix} A & B \\ B & D \end{bmatrix} \begin{bmatrix} \varepsilon_0 \\ k \end{bmatrix} \tag{18}$$

which can be expanded as follows [17]:

$$\begin{bmatrix} N_x \\ N_y \\ N_{xy} \\ M_x \\ M_y \\ M_{xy} \end{bmatrix} = \begin{bmatrix} A_{11} & A_{12} & A_{16} & B_{11} & B_{12} & B_{16} \\ A_{21} & A_{22} & A_{26} & B_{21} & B_{22} & B_{26} \\ A_{61} & A_{62} & A_{66} & B_{61} & B_{62} & B_{66} \\ B_{11} & B_{12} & B_{16} & D_{11} & D_{12} & D_{16} \\ B_{21} & B_{21} & B_{26} & D_{21} & D_{22} & D_{26} \\ B_{61} & B_{62} & B_{66} & D_{61} & D_{62} & D_{66} \end{bmatrix} \begin{bmatrix} \varepsilon_{0,x} \\ \varepsilon_{0,y} \\ \gamma_{0,xy} \\ k_x \\ k_y \\ k_{xy} \end{bmatrix} \tag{19}$$

where the *ABD* matrix coefficients can be obtained as [17]:

$$A_{ij} = \sum_{k=1}^{N} (Q_{ij})_k (z_k - z_{k-1}) \tag{20a}$$

$$B_{ij} = \frac{1}{2} \sum_{k=1}^{N} (Q_{ij})_k (z_k^2 - z_{k-1}^2) \tag{20b}$$

$$D_{ij} = \frac{1}{3} \sum_{k=1}^{N} (Q_{ij})_k (z_k^3 - z_{k-1}^3) \tag{20c}$$

System of PDE's given by Eqs. (21)-(23) are the governing equations of the sandwich panel which are derived by substitution of Eqs. (20a)-(20c) into Eqs. (15)-(17).

$$\begin{aligned} & \left(A_{11,x} + A_{16,y}\right)u_{0,x} + \left(A_{16,x} + A_{66,y}\right)u_{0,y} + \left(A_{16,x} + A_{66,y}\right)v_{0,x} + \left(A_{12,x} + A_{26,y}\right)v_{0,y} - \left(B_{11,x} + B_{16,y}\right)w_{0,xx} \\ & -2\left(B_{16,x} + B_{66,y}\right)w_{0,xy} - \left(B_{12,x} + B_{26,y}\right)w_{0,yy} + A_{11}u_{0,xx} + 2A_{16}u_{0,yy} + A_{66}u_{0,yy} + A_{16}v_{0,xx} \\ & + \left(A_{12} + A_{66}\right)v_{0,xy} + A_{26}v_{0,yy} - B_{11}w_{0,xxx} - 3B_{16}w_{0,xxy} - \left(B_{12} + 2B_{66}\right)w_{0,xyy} - B_{26}w_{0,yyy} = 0 \end{aligned} \tag{21}$$

$$\left(A_{16,x}+A_{12,y}\right)u_{0,x}-\left(A_{66,x}+A_{26,y}\right)u_{0,y}+\left(A_{66,x}+A_{26,y}\right)\upsilon_{0,x}+\left(A_{26,x}+A_{22,y}\right)\upsilon_{0,y}-\left(B_{16,x}+B_{12,y}\right)w_{0,xx}$$

$$-2\left(B_{66,x}+B_{26,y}\right)w_{0,xy}-\left(B_{26,x}+B_{22,y}\right)w_{0,yy}+A_{16}u_{0,xx}+\left(A_{12}+A_{66}\right)u_{0,xy}+A_{26}u_{0,yy}+A_{66}\upsilon_{0,xx} \tag{22}$$

$$+2A_{26}\upsilon_{0,xy}+A_{22}\upsilon_{0,yy}-B_{16}w_{0,xxx}-\left(B_{12}+2B_{66}\right)w_{0,xxy}-3B_{26}w_{0,xyy}-B_{22}w_{0,yyy}=0$$

$$\left(B_{11,xx}+2B_{16,xy}+B_{12,yy}\right)u_{0,x}+\left(B_{16,xx}+2B_{66,xy}+B_{26,yy}\right)u_{0,y}+\left(B_{16,xx}+2B_{66,xy}+B_{26,yy}\right)\upsilon_{0,x}$$

$$+\left(B_{12,xx}+2B_{26,xy}+B_{22,yy}\right)\upsilon_{0,y}-\left(D_{11,xx}+2D_{16,xy}+D_{12,yy}\right)w_{0,xx}-2\left(D_{16,xx}+4D_{66,xy}+2D_{26,yy}\right)w_{0,xy}$$

$$-\left(D_{12,xx}+2D_{26,xy}+D_{22,yy}\right)w_{0,yy}+2\left(B_{11,x}+B_{16,y}\right)u_{0,xx}+2\left(2B_{16,x}+B_{66,y}\right)u_{0,xy}+2\left(B_{66,x}+B_{26,y}\right)$$

$$+2\left(B_{16,x}+B_{26,y}\right)\upsilon_{0,xx}+2\left(B_{12,x}+2B_{26,y}+B_{66,x}\right)\upsilon_{0,xy}+2\left(B_{26,x}+B_{22,y}\right)\upsilon_{0,yy}-2\left(D_{11,x}+D_{16,y}\right)w_{0,xxx} \tag{23}$$

$$-\left(6D_{16,x}+2D_{12,y}+4D_{66,y}\right)w_{0,xxy}-\left(2D_{12,x}+6D_{26,y}+4D_{66,x}\right)w_{0,xxy}+3B_{16}u_{0,xxy}+\left(2B_{66}+B_{12}\right)u_{0,xyy}$$

$$+B_{26}u_{0,yyy}+B_{16}\upsilon_{0,xxx}+\left(B_{12}+2B_{66}\right)\upsilon_{0,xxy}+3B_{26}\upsilon_{0,xyy}+B_{22}\upsilon_{0,yyy}-D_{11}w_{0,xxxx}-4D_{16}w_{0,xxxy}$$

$$-\left(2D_{12}+4D_{66}\right)w_{0,xxyy}-4D_{26}w_{0,xyyy}-D_{22}w_{0,yyyy}+p=0$$

where the second indeces are devoted to local drivatives.

As can be seen in Eqs. (21)-(23) all the derivatives of stiffness coefficients are taken into account, unlike the work done by Li and Cheng [5] in which the first-order derivatives of stiffness coefficients are ignored in the third equilirium equation.

2.4 Solution

The boundary conditions of the plate is assumed to be simply supported on all edges. By applying Galerkin's method, the solution to system of PDE's (Eqs. (21)-(23)) can be obtained. Eqs. (24)-(26) show the shape functions which satisfy the simply supported boundary conditions of the problem [18].

$$\Phi_{mn}\left(x,y\right)=\sum_m\sum_n\cos\left(\frac{m\pi}{a}x\right)\sin\left(\frac{n\pi}{b}y\right) \tag{24}$$

$$X_{mn}\left(x,y\right)=\sum_m\sum_n\sin\left(\frac{m\pi}{a}x\right)\cos\left(\frac{n\pi}{b}y\right) \tag{25}$$

$$\Psi_{mn}\left(x,y\right)=\sum_m\sum_n\sin\left(\frac{m\pi}{a}x\right)\sin\left(\frac{n\pi}{b}y\right) \tag{26}$$

The applied lateral pressure load can be defined as follows:

$$p=\sum_{m=1}^{\infty}\sum_{n=1}^{\infty}p_{mn}\sin\left(\frac{m\pi}{a}x\right)\sin\left(\frac{n\pi}{b}y\right) \tag{27}$$

Then the displacement components can be written in terms of shape functions as follows:

$$u_0=U_{mn}\Phi_{mn}\left(x,y\right) \tag{28a}$$

$$\upsilon_0=V_{mn}X_{mn}\left(x,y\right) \tag{28b}$$

$$w_0=W_{mn}\Psi_{mn}\left(x,y\right) \tag{28c}$$

The system of PDE's in Eqs. (21)-(23) can be rewritten in a concise form as follows:

$$\begin{bmatrix} L_{ij} \end{bmatrix} \begin{bmatrix} u_0 \\ \upsilon_0 \\ w_0 \end{bmatrix} = \begin{bmatrix} 0 \\ 0 \\ p \end{bmatrix} \quad i,j=1,2,3 \tag{29}$$

Then Galerkin's method is applied as:

$$\iiint\limits_{V} L_1\left(u_0,\upsilon_0,w_0\right)\Phi_{mn}\left(x,y\right)dxdydz = 0 \tag{30}$$

$$\iiint\limits_{V} L_2\left(u_0,\upsilon_0,w_0\right)X_{mn}\left(x,y\right)dxdydz = 0 \tag{31}$$

$$\iiint\limits_{V} L_3\left(u_0,\upsilon_0,w_0\right)\Psi_{mn}\left(x,y\right)dxdydz + \iiint\limits_{V} p\Psi_{mn}\left(x,y\right)dxdydz = 0 \tag{32}$$

Linear solution to the static bending problem, considering uniform lateral pressure can be expressed as the following form:

$$\begin{bmatrix} u_0 \\ \upsilon_0 \\ w_0 \end{bmatrix} = \begin{bmatrix} k_{11} & k_{12} & k_{13} \\ k_{21} & k_{22} & k_{23} \\ k_{31} & k_{32} & k_{33} \end{bmatrix}^{-1} \begin{bmatrix} 0 \\ 0 \\ \dfrac{4p}{mn\pi^2} \end{bmatrix} \tag{33}$$

which the *k* matrix coefficients are given in the Appendix.

3 VERIFICATION OF RESULTS

In order to investigate the validity of the present analytical solution, several comparisons have been carried out. The present analytical results are compared with the few reported in the literature. There are numerical results obtained by Crisfield [3] who solved the elastostatic problem of isotropic plates with voids using equivalent plate analogy. The same problem has been investigated by Takabatake [3] using exact material modeling. For further validation, a finite element modeling has been developed by ABAQUS software using C3D8R elements.

Geometrical characteristics for two types of isotropic plates with voids are given in Table 1., and the Poisson's ratio v is considered to be 0.17. Non-dimensional deflection and bending moment for the type1 plate are shown in Figs. 3 and 4, respectively. D_0 is the flexural rigidity of the structure without voids which is given by $Eh^3/12\left(1-\upsilon^2\right)$.

The horizontal axis is the non-dimensional length of the plate. Numerical values are evaluated on coordinates $y=b/2$ and $0\leq x \leq a$, The present analytical results for deflection and bending are equal to those obtained by Takabatake, because the Takabateke's solution is a special case of the present general solution.
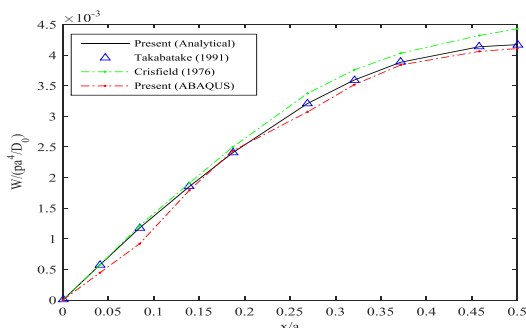
Fig.3
Non-dimensional deflection for the isotropic type A plate.
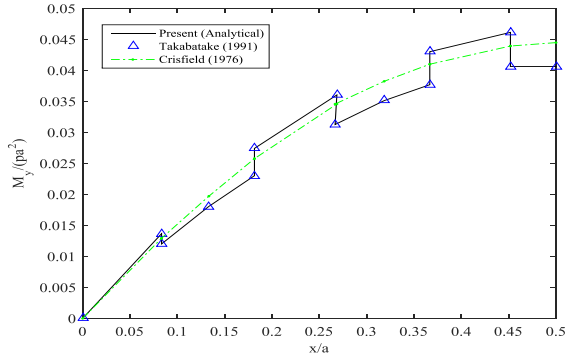
Fig.4
Non-dimensional momentum for the isotropic type A plate.

Table 1
Geometrical characteristics for two types of isotropic plates

Type	Plane	Section	$\dfrac{h_c}{h_T}$	$\dfrac{c}{a}$	$\dfrac{d}{b}$	$\dfrac{b}{a}$
A			0.5	0.1	0.5	1
B			0.5	0.1	0.1	1
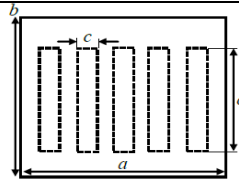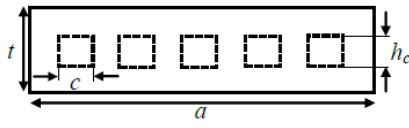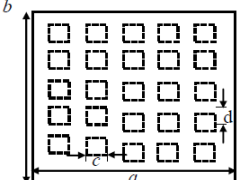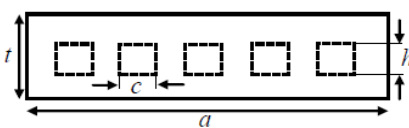
Results of non-dimensional deflection and bending moment for the isotropic type B plate are shown in Figs. 5 and 6, respectively. For the type B plate, the difference between Crisfield and FEM results has become greater than type A plate in both deflection and bending moment values, so it can be concluded that the equivalent plate analogy becomes inefficient as the number of voids increase.

As can be seen in Fig. 3 and Fig. 5 analytical results for deflection are in better agreement with FEM than the Crisfiled's curve. In fact, the equivalent plate analogy overpredicts the deflections.

Unlike the analytical results of deflection that the curve slope gradually decreases from edge to the middle of the plate, the FEM curve slope increases and decreases alternatively. This alternation becomes negligible gradually by approaching to the middle of the plate (see Fig. 3 and 5). The reason of these variations is the local variation of stiffness due to the existence of voids. Since the type B plate possesses more uniform distribution of voids, the FEM deflection curve shows lower slope variations in comparison with the type A plate.
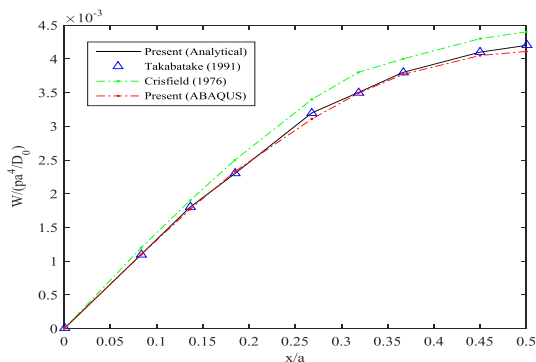
Fig.5
Non-dimensional deflection for the isotropic type B plate.
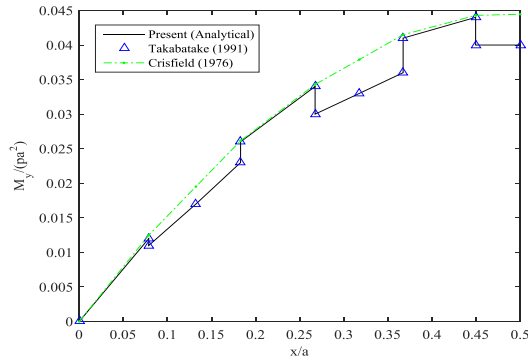
Fig.6
Non-dimensional momentum for the isotropic type B plate.

4   PARAMETRIC STUDIES

In order to evaluate the deflection behavior of orthogonally-rib stiffened sandwich panels, many parametric studies has been done herein. A simply supported edge composite sandwich panel with foam-filled orthogonally rib-stiffened core subjected to uniform lateral pressure is considered

   Unless otherwise stated, the geometry and material properties are used as the basic values presented in Tables 2 and 3 for all of the parametric studies.

Table 2
Basic material properties.

Material [5]	Region	$E_{11} [GPa]$	$E_{22} [GPa]$	$G_{12} [GPa]$	v_{12}
Fiber reinforced polymer	Ribs and face sheets	25.2	7.5	2.4	0.32
Foam (filler)	Cells	7.2	7.2	2.707	0.33

Table 3
Basic geometry properties.

Dimensions	$a=b=900mm, c=d, m_x=n_y=1$
Lay up	[0]

Volume fraction of filler material can be defined as:

$$R = m_x n_y \frac{c \times d}{a \times b} \times 100 \tag{34}$$

   Three types of structures with different sandwich constructions are considered as shown in Table 4., which are used in the parametric studies. The parameter *t* is total thickness of the structure which is equal to 45*mm* every where, unless otherwise stated.

Table 4
Sandwich types.

Ply name	Thickness		
	Type 1	Type 2	Type 3
Upper face sheet	0	0.1*t*	0.05*t*
Core	*t*	0.9*t*	0.9*t*
Lower face	0	0	0.05*t*
Sandwich configuration			

Since the present analytical theory gives acceptable results only in linear elastic deformation conditions, the applied load value is chosen such that the deflection to thickness ratio is not more than 0.5. All of the results are obtained at the center of the structure ($a/2,b/2,0$) where the maximum deflection occures.

Execept the section 4.1 where the ABAQUS results are reported to examin the accuracy of the analytical solution, in other sections the results are obtained using analytical solution.

It should be noted that in sections 4.1 to 4.4 the mathematical model with two material regions is used because the structure is made of laminated composite, while in the section 4.5 the mathematical model with four material regions is used for the filament wound structure.

4.1 Effect of filler region size

In order to examin the accuracy of analytical solution as the filler region size changes, a finite element simulation has been performed by ABAQUS using S4R elements.

Assuming $m_x = n_y = 1$, the results of W_{max} / t ratio for the three types of sandwich structures introduced in Table 4., are given in Tables (5-7). The maximum discrepancy equal to 8.88% between analytical and FEM results is observed in the second row of Tables (5-7) where R is equal to 10 and the size of filler region is small. By increasing the filler region size from $R=10\%$ to $R=100\%$ the discrepancy value is gradually decreased.

Making comparison among Tables (5-7) indicates that the discrepancies are decreased by adding face sheets and making sandwich structure. The main reason is that in a sandwich structure, the more normal force will be tolerated by the face sheets and the middle layers are to tolerate more shear force. Since the classical lamination theory ignores in plane shear forces, the discrepancy is decreased by adding face sheets.

Table 5

W_{max} / t ratio results for the type 1 structure ($p=500\ kPa$, $m_x=n_y=1$).

R (%)	Theory	ABAQUS	Discrepancy(%)
0	0.3228	0.3313	2.5730
10	0.3680	0.4039	8.8806
20	0.4081	0.4428	7.8392
30	0.4405	0.4678	5.8350
40	0.4640	0.4834	4.0067
50	0.4790	0.4922	2.6871
60	0.4869	0.4963	1.8948
70	0.4896	0.4971	1.5048
80	0.4889	0.4956	1.3600
90	0.4862	0.4928	1.3380
100	0.4827	0.4892	1.3378

Table 6

W_{max} / t ratio results for the type 2 structure ($p=500\ kPa$, $m_x=n_y=1$).

R (%)	Theory	ABAQUS	Discrepancy(%)
0	0.3228	0.3313	2.5730
10	0.3570	0.3838	6.9713
20	0.3865	0.4126	6.3232
30	0.4099	0.4312	4.9293
40	0.4270	0.4430	3.5969
50	0.4383	0.4499	2.5896
60	0.4445	0.4533	1.9535
70	0.4469	0.4542	1.6222
80	0.4467	0.4535	1.4873
90	0.4451	0.4516	1.4549
100	0.4427	0.4492	1.4450

Table 7
W_{max}/t ratio results for the type 3 structure (p=500 kPa, m_x=n_y=1).

R (%)	Theory	ABAQUS	Discrepancy(%)
0	0.3228	0.3313	2.5730
10	0.3556	0.3793	6.2422
20	0.3830	0.4052	5.4733
30	0.4040	0.4217	4.1958
40	0.4187	0.4320	3.0860
50	0.4278	0.4379	2.3034
60	0.4326	0.4407	1.8314
70	0.4343	0.4413	1.5881
80	0.4340	0.4405	1.4866
90	0.4325	0.4389	1.4584
100	0.4303	0.4367	1.4468

The FEM meshed model created in ABAQUS software is shown in Fig. 7(a), and the deflection contour of the one is shown in Fig. 7(b).
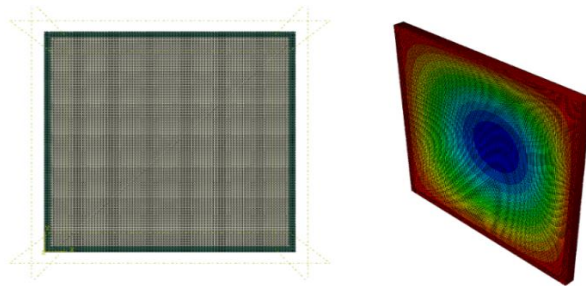
Fig.7
The type 1 structure (R=90%, m_x=n_y=1): (a) FEM model, (b) FEM deflection countour.

4.2 Effect of load

In order to study the effect of lateral pressure load value, the type 1 structure is considered. Assuming m_x= n_y=1, analytical results are plotted for R values from 0 to 70% in Fig. 8.
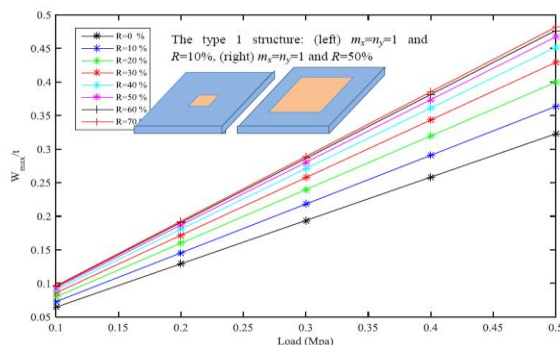
Fig.8
Variations of W_{max}/t ratio versus load for type1 structure with different R values (m_x=n_y=1).

The stiffness of total structure can be obtained from the slope of lines to the vertical axis. As shown in Fig. 8, the structure becomes stiffer by decreasing the filler volume. Furthermore when the filler region boundaries approaches the plate boundaries (for R values higher than about 60%), the variation of stiffness become minimum.

4.3 Effect of thickness

Assuming m_x=n_y=1, for the type1 structure the effect of thickness to width ratio is investigated in Fig. 9. According to the results, the deflection values are decreased by increasing the thickness of structure. For t/a values bigger than about 0.03, the deflection of the plate becomes almost independent of filler material volume which means that the thickness parameter has more dominant effect on the deflection in comparison with the parameter R.
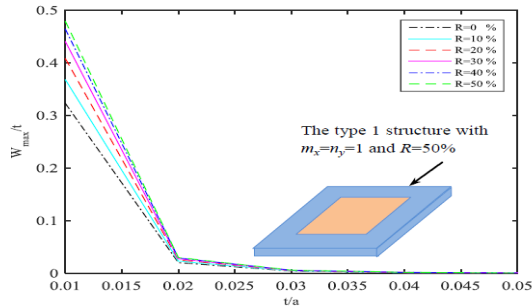
Fig.9
Variations of W_{max}/t ratio versus t/a for the type 1 structure ($p=0.8\ kPa$, $m_x=n_y=1$).

4.4 Effect of number of cells

Number of cells mainly affects the structure deflection behavior. Increasing number of cells for the type 3 structure considering different R values is what has been done here. According to the results in Fig. 10 for m_x or n_y greater than 4, the maximum deflection becomes almost independant to the number of cells and R values, because high number of voids bring more integrity for the structure.
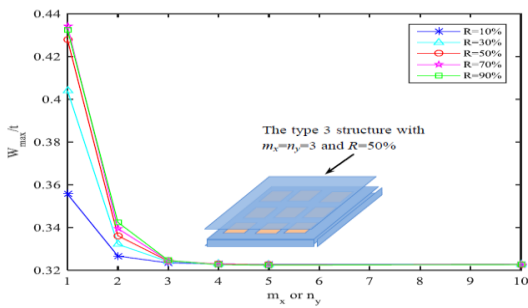
Fig.10
Variations of W_{max}/t ratio versus m_x or n_y for the type 3 structure ($p=500\ kPa$).

4.5 Effect of fabrication method

The purpose of this section is to evaluate the effect of fabrication method on the maximum deflection of the types (1-3) structures. Volume fraction of filler material is considered to be $R=90\%$ in this study.

Orthogonally rib-stiffened filament wound structures include four material regions and it is necessary to use the developed material modeling given by Eq. (3). A cell surrounded by unidirectional ribs is specified in a red cubic frame (see Fig. 11), which can be considered as the unit cell of an orthogrid filament wound plate. In order to observe the variation of stiffness in a foam filled orthogonally rib-stiffened filament wound plate, the ABD coefficients distribution of the one cell surrounded by unidirectional ribs are illustrated in Figs. 12 and 13.
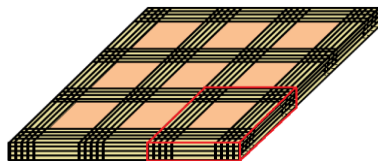
Fig.11
One cell surrounded by unidirectional ribs.
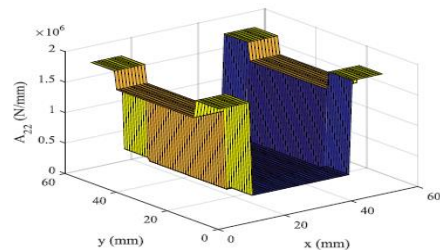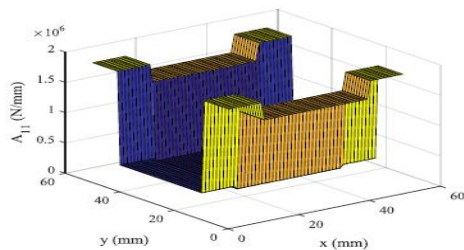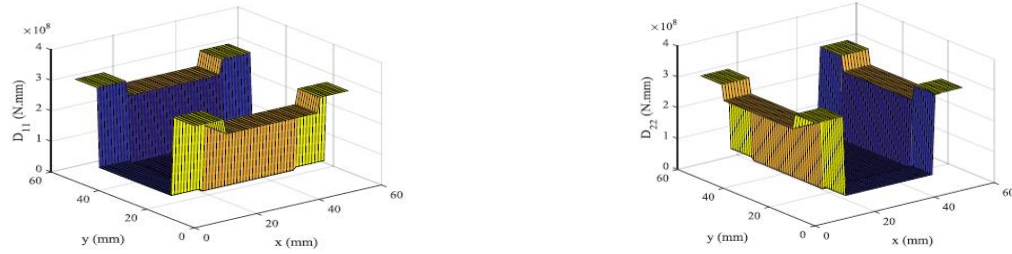
Fig.12
Distribution of: (a) A_{11}, (b) A_{22}, (c) D_{11}, and (d) D_{22} on the plane of one cell surrounded by unidirectional ribs.
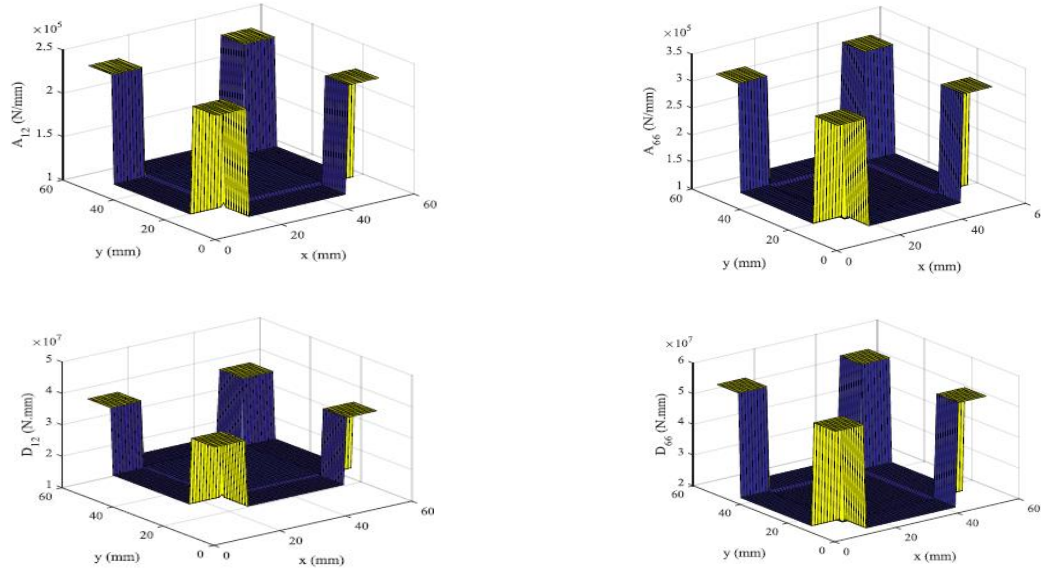
Fig.13
Distribution of: (a) A_{12}, (b) A_{66}, (c) D_{12}, and (d) D_{66} on the plane of one cell surrounded by unidirectional ribs.

It is considered that the rib regions are made of two layers of GFRP with 40% fiber volume fraction and the inresection regions are made of four layers of GFRP with 75% fiber volume fraction (see Table 8) and foam material properties (see Table 2) are devoted to the internal cell. The Number of layers considered for rib and intersection regions are 4 and 8 respectively. The material properties reported in Table 8 is obtained from pure Glass fiber and Epoxy resin properties using micromechanical rules [17].

Table 8
Orthotropic properties of GFRP with fiber volume fractions of 40% and 75%.

Material	$E_{11}\,[GPa]$	$E_{22}\,[GPa]$	$G_{12}\,[GPa]$	v_{12}
GFRP (v_f=40%)	36.04	9.03	2.85	0.28
GFRP (v_f=75%)	64.6	23.8	7.31	0.23

Based on the diagrams in Fig. 12, the following relations exist:

$$\left(A_{11},D_{11}\right)_{filler} = \left(A_{22},D_{22}\right)_{filler} \tag{35a}$$

$$\left(A_{11},D_{11}\right)_{intersection} = \left(A_{22},D_{22}\right)_{intersection} \tag{35b}$$

$$\left(A_{11},D_{11}\right)_{vertical\ ribs} = \left(A_{22},D_{22}\right)_{vertical\ ribs} \tag{35c}$$

$$\left(A_{11},D_{11}\right)_{horizental\ ribs} = \left(A_{22},D_{22}\right)_{horizental\ ribs} \tag{35d}$$

According to Fig. 13 diagrams, the maximum value of coefficients A_{12}, A_{66}, D_{12} and D_{66} are obtianed at the intersection regions, which means that these regions are the most susceptible regions creating extension-extension, shear-shear, bending-bending and twist-twist couplings.

Considering laminated and filament wound fabrication methods for the types (1-3) structures, the maximum deflection results are given in Fig. 14. The laminated structures with $[0.90]_S$ and $[0.90]_2$ stacking sequences are considered to be made of GFRP with 40% fiber volume fraction (Table 8). The face sheets used for all three types of structures are considered to be made of GFRP with 40% fiber volume fraction and [0] stacking sequence (Table 8).

According to results presented in Figs. 14 (a-c) For structures including more than one cell, the maximum deflection observed for the filament wound structure is lower than the two other structures. This is due to the fact that the filament wound structure includes intersection regions with high stiffness.

(a)

(b)

(c)
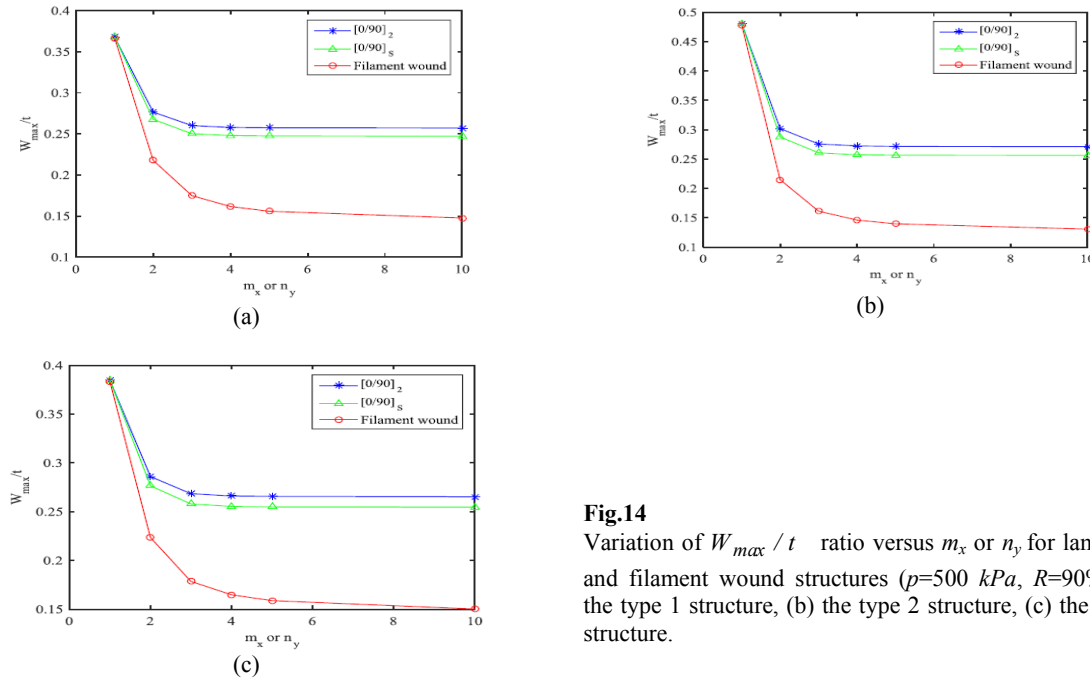
Fig.14

Variation of W_{max} / t ratio versus m_x or n_y for laminated and filament wound structures (p=500 kPa, R=90%): (a) the type 1 structure, (b) the type 2 structure, (c) the type 3 structure.

As shown in Figs. 14(a-c), as the number of cells increases, the structure possesses uniform structural stiffness and the variation of w_{max}/t ratio converges to a constant value. For the filament wound structure, the w_{max}/t ratio convergence is faster in the type 1 structure (see Fig. 14(a)) in comparison with the two other ones. In another word, the structures with face sheets like the type 2 and 3 ones possesses the uniform structural stiffness in higher number of cells.

By making comparison between the laminated structure with $[0.90]_2$ stacking sequence and the filament wound one, it can be conluded that filament winding process can decsrease the maximum deflection by 51.8%, 42.6% and 43.4% for the types (1-3) structures, respectively.

5   CONCLUSIONS

Using a developed mathematical modeling in conjunction with classical lamination theory, a general analytical solution is presented for static bending analysis of composite sandwich panels with foam filled orthogonally rib-stiffened core. The current model is governed by a system of three PDEs which is solved by Galerkin's method. Analytical results have been compared with the few in literature, and FEM results obtained by ABAQUS software and the results are in good agreement. The main results obtained by parametric studies can be summarized as:
1) By studying the effect of filler region size, a maximum discrepancy of 8.88% between analytical and FEM results achived which corresponds to the type 1 structure with the filler region size of R=10%.
2) The effect of R value on the maximum deflection of structure has been observed considerable when the total thickness is decreased.

3) Studying variation of maximum deflection by increasing the load shows that the structure becomes stiffer by decreasing filler volume.
4) By increasing the number of cells ($m_x=n_y> 4$), the structure possesses uniform structural stiffness and the maximum deflection becomes almost independant to the number and volume fraction of cells.
5) Investigating the effect of fabrication method, shows that the filament wound structure demonstrate lower deflection in comparison with the laminated ones because the intersection regions are very stiff. Furthermore it is concluded the using the filament wound structures instead of the laminated ones the maximum deflection can be decreases up to 51.8%.

The main aim of this study was to present a general solution procedure for static bending analysis of laminated and filament wound orthogrid structures. Structures stiffened by angle ribs can be modeled by extension of the present method in the future.

APPENDIX

$$k_{11} = \int_0^b\int_0^a\int_{-h/2}^{h/2} \left(\left(A_{11,x}+A_{16,y}\right)u_{0,x} + \left(A_{16,x}+A_{66,y}\right)u_{0,y} + A_{16}u_{0,xx} + \left(A_{12}+A_{66}\right)u_{0,xy} + A_{26}u_{0,yy}\right)\Phi_{mn}(x,y)dxdydz \tag{A.1}$$

$$k_{12} = \int_0^b\int_0^a\int_{-h/2}^{h/2} \left(\left(A_{16,x}+A_{66,y}\right)\upsilon_{0,x} + \left(A_{12,x}+A_{26,y}\right)\upsilon_{0,y} + A_{16}\upsilon_{0,xx} + \left(A_{12}+A_{66}\right)\upsilon_{0,xy} + A_{260,yy}\right)X_{mn}(x,y)dxdydz \tag{A.2}$$

$$k_{13} = \int_0^b\int_0^a\int_{-h/2}^{h/2} \left(-\left(B_{11,x}+B_{16,y}\right)w_{0,xx} - 2\left(B_{16,x}+B_{66,y}\right)w_{0,xy} - \left(B_{12,x}+B_{26,y}\right)w_{0,yy} - B_{11}w_{0,xxx} - 3B_{16}w_{0,xxy}\right.$$
$$\left. -\left(B_{12}+2B_{66}\right)w_{0,xyy} - B_{26}w_{0,yyy}\right)\Psi_{mn}(x,y)dxdydz \tag{A.3}$$

$$k_{21} = \int_0^b\int_0^a\int_{-h/2}^{h/2} \left(\left(A_{16,x}+A_{12,y}\right)u_{0,x} - \left(A_{66,x}+A_{26,y}\right)u_{0,y} + A_{16}u_{0,xx} + \left(A_{12}+A_{66}\right)u_{0,xy} + A_{26}u_{0,yy}\right)\Phi_{mn}(x,y)dxdydz \tag{A.4}$$

$$k_{22} = \int_0^b\int_0^a\int_{-h/2}^{h/2} \left(\left(A_{66,x}+A_{26,y}\right)\upsilon_{0,x} + \left(A_{26,x}+A_{22,y}\right)\upsilon_{0,y} + A_{66}\upsilon_{0,xx} + 2A_{26}\upsilon_{0,xy} + A_{22}\upsilon_{0,yy}\right)X_{mn}(x,y)dxdydz \tag{A.5}$$

$$k_{23} = \int_0^b\int_0^a\int_{-h/2}^{h/2} \left(-\left(B_{16,x}+B_{12,y}\right)w_{0,xx} - 2\left(B_{66,x}+B_{26,y}\right)w_{0,xy} - \left(B_{26,x}+B_{22,y}\right)w_{0,yy} - B_{16}w_{0,xxx}\right.$$
$$\left. -\left(B_{12}+2B_{66}\right)w_{0,xxy} - 3B_{26}w_{0,xyy} - B_{22}w_{0,yyy}\right)\Psi_{mn}(x,y)dxdydz \tag{A.6}$$

$$k_{31} = \int_0^b\int_0^a\int_{-h/2}^{h/2} \left(\left(B_{11,xx}+B_{16,xy}+B_{12,yy}\right)u_{0,x} + \left(B_{16,xx}+2B_{66,xy}+B_{26,yy}\right)u_{0,xy} + 2\left(B_{11,x}+B_{16,y}\right)u_{0,xx}\right.$$
$$+2\left(2B_{16,x}+B_{66,y}+B_{12,y}\right)u_{0,xy} + 2\left(B_{66,x}+B_{26,y}\right)u_{0,yy} + B_{11}u_{0,xxx} + 3B_{16}u_{0,xxy}$$
$$\left. +\left(2B_{66}+B_{12}\right)u_{0,xyy} + B_{26}u_{0,yyy}\right)\Phi_{mn}(x,y)dxdydz \tag{A.7}$$

$$k_{32} = \int_0^b\int_0^a\int_{-h/2}^{h/2} \left(\left(B_{16,xx}+2B_{66,xy}+B_{26,yy}\right)\upsilon_{0,x} + \left(B_{12,xx}+B_{26,xy}+B_{22,yy}\right)\upsilon_{0,y} + 2\left(B_{16,x}+B_{66,y}\right)\upsilon_{0,xx}\right.$$
$$+2\left(B_{12,xx}+2B_{26,y}+B_{66,x}\right)\upsilon_{0,xy} + 2\left(B_{26,x}+B_{22,y}\right)\upsilon_{0,yy} + B_{16}\upsilon_{0,xxx} + \left(B_{12}+2B_{66}\right)\upsilon_{0,xxy}$$
$$\left. +3B_{26}\upsilon_{0,xyy} + B_{22}\upsilon_{0,yyy}\right)X_{mn}(x,y)dxdydz \tag{A.8}$$

$$k_{33} = \int_0^b \int_0^a \int_{-h/2}^{h/2} \left(-\left(D_{11,xx} + 2D_{16,xy} + B_{12,yy}\right)w_{0,xx} - \left(2D_{16,xx} + 4D_{66,xy} + 2D_{26,yy}\right)w_{0,xy} - \left(D_{12,xx} + 2D_{26,xy} + D_{22,yy}\right)w_{0,yy} \right.$$

$$-2\left(D_{11,x} + D_{16,y}\right)w_{0,xxx} - 2\left(D_{11,x} + D_{16,y}\right)w_{0,xxx} - \left(6D_{16,x} + 2D_{12,y} + 4D_{66,y}\right)w_{0,xxy} - \left(2D_{12,x} + 6D_{26,y} + 4D_{66,x}\right)w_{0,xyy}$$

$$-2\left(D_{22,y} + D_{26,x}\right)w_{0,yyy} - D_{11}w_{0,xxxx} - \left(2D_{12} + 4D_{66}\right)w_{0,xxyy} - 4D_{26}w_{0,xyyy} - D_{22}w_{0,yyyy} \left. \right)\Psi_{mn}(x,y)dxdydz$$

(A.9)

REFERENCES

[1] Yetram A.L., Brown C.J., 1985, The elastic stability of square perforated plates, *Computers & Structures* **21**: 1267-1272.

[2] Choi S., Jeong K.H., Kim T.W., Kim K.S., Park K.B., 1998, Free vibration analysis of perforated plates using equivalent elastic properties, *Journal of the Korean Nuclear Society* **30**: 416-423.

[3] Takabatake H., 1991, Static analyses of elastic plates with voids, *International Journal of Solids and Structures* **28**: 179-196.

[4] Rezaeepazhand J., Jafari M., 2005, Stress analysis of perforated composite plates, *Composite Structures* **71**: 463-468.

[5] Li G., Cheng J., 2012, A generalized analytical modeling of grid stiffened composite structures, *Composite Structures* **94**: 1117-1127.

[6] Huang L., Sheikh A.H., Ng C.T., Griffith M.C., 2015, An efficient finite element model for buckling analysis of grid stiffened laminated composite plates, *Composite Structures* **122**: 41-50.

[7] Wodesenbet E., Kidane S., Pang S.S., 2003, Optimization for buckling loads of grid stiffened composite panels, *Composite Structures* **60**: 159-169.

[8] Legault J., Mejdi A., Atalla N., 2011, Vibro-acoustic response of orthogonally stiffened panels: The effects of finite dimensions, *Journal of Sound and Vibration* **330**: 5928-5948.

[9] Priyadharshani S.A., Prasad A.M., Sundaravadivelu R., 2017, Analysis of GFRP stiffened composite plates with rectangular cutout, *Composite Structures* **169**: 42-51.

[10] Nemeth M.P., 2011, *A Treatise on Equivalent-Plate Stiffnesses for Stiffened Laminated-Composite Plates and Plate-Like Lattices*, NASA TP, Virginia.

[11] Weber M.J., Middendorf P., 2014, Semi-analytical skin buckling of curved orthotropic grid-stiffened shells, *Composite Structures* **108**: 616-624.

[12] Ovesy H.R., Fazilati J., 2012, Buckling and free vibration finite strip analysis of composite plates with cutout based on two different modeling approaches, *Composite Structures* **94**: 1250-1258.

[13] Qin X.C., Dong C.Y., Wang F., Qu X.Y., 2017, Static and dynamic analyses of isogeometric curvilinearly stiffenedplates, *Applied Mathematical Modelling* **45**: 336-364 .

[14] Azhari M., Shahidi A.R., Saadatpour M.M., 2005, Local and post local buckling of stepped and perforated thin plates, *Applied Mathematical Modelling* **29**: 633-652.

[15] John Wilson A., Rajasekaran S., 2014, Elastic stability of all edges simply supported, stepped and stiffened rectangular plate under Biaxial loading, *Applied Mathematical Modelling* **38**: 479-495.

[16] Vasiliev V.V., Barynin V.A., Razin A.F., 2012, Anisogrid composite lattice structures – development and aerospace applications, *Composite Structures* **94**: 1117-1127.

[17] Kaw A.K., 2006, *Mechanics of Composite Materials*, CRC Press, Taylor & Francis Group, Boca Raton,

[18] Whitney J.M., 1987, *Structural Analysis of Laminated Anisotropic Plates*, Technomic Publishing Company, Pennsylvania.